CO2 TRANSCRITICAL TURBINES STATOR OPTIMIZATION FOR REFRIGERATION APPLICATIONS

Renaud Saugnac, Egoi Ortego Sampedro, Chakib Bouallou

Proceedings of ASME Turbo Expo 2024
Turbomachinery Technical Conference and Exposition
GT2024
June 24-28, 2024, London, United Kingdom

GT2024-127501

CO2 TRANSCRITICAL TURBINES STATOR OPTIMIZATION FOR REFRIGERATION APPLICATIONS

Renaud Saugnac[1], Egoï Ortego Sampedro[1], Chakib Bouallou[1]

[1]Mines Paris, PSL University, CES, 60 Bd St Michel 75006 Paris, France

ABSTRACT

The main objective of this work presented in the paper is to perform an optimization of the stator nozzle. This is done using a 1D two-phase metastable model which includes a transitional interface area formulation, the Aleksandrov interface heat transfer coefficient and Schiller-Naumann interface drag model. The optimization is based on the research of an optimal pressure profile defined by Bezier curves leading to an optimal cross-sectional area profile. Various types of linear constrained optimization algorithms were explored. The results show that for inlet operating conditions close to critical point of CO_2, the maximum efficiency that can be attained is always higher than at lower inlet temperature conditions. The obtained optimal nozzle profiles should be tested in subsequent experimental work in order to evaluate the performance of the method.

Keywords: CO_2 two phase flow, 1D nozzle modeling

NOMENCLATURE

Symbols

α	volume fraction
A	nozzle section, m²
p	pressure, Pa
u	velocity, m/s
h	enthalpy, J/kg
d	tube diameter, m
ρ	density, kg/m^3
Γ	mass transfer term, kg/m^3. s
F	interfacial drag force, kg.m/s²
T	temperature, K
A_i	interface area, m²
C_D	drag coefficient
k	thermal conductivity, W/m.K
N_b	bubble number, m^{-3}
N_d	droplet number, m^{-3}
U	overall heat-transfer coefficient, W/m².K
Re	Reynolds number
Pr	Prandtl number
Nu	Nusselt number
Ja	Jakob number
Pe	Péclet number
μ	dynamic viscosity, Pa.s
C_p	specific-heat capacity, J/kg.K
$\dot{m}$	mass-flow rate, kg/s
$\dot{x}$	mass fraction
D	diameter, m
$D_{T,l}$	thermal diffusivity, m²/s
$\mathfrak{H}$	heat transfer coefficient, W/m²K
ξ	friction factor
x	nozzle position, m
l_c	interfacial characteristic length, m
N	number of nodes
j	iteration index

Subscripts

ex	exchanged phase
l	liquid
v	vapour
isen	isentropic
mix	mixing
in	inlet
out	outlet
f	frictional
nzl	nozzle
exp	experimental
ini	initialized
CFD	Computational Fluid Dynamics

1. INTRODUCTION

The global temperature increase as well as the increasingly frequent heat waves will result in the increasing use of air conditioning. Improving the efficiency of refrigeration systems is therefore a crucial issue for limiting constraints on the management and supply of electricity in the future. In addition, current regulatory developments leave room, among other fluids, for natural refrigeration fluids. In this context, the use of CO_2 has many advantages. However, its thermodynamic efficiency is relatively low and its use is currently limited to countries with a temperate climate. Several improvement ways exist. One of the major items of losses is the expansion valve, it can be responsible of 30% of the exergy losses of the refrigeration system [1]. A two-phase turbine would make it possible to recover these losses by producing work and would also increase the refrigeration capacity of the system figure (1).

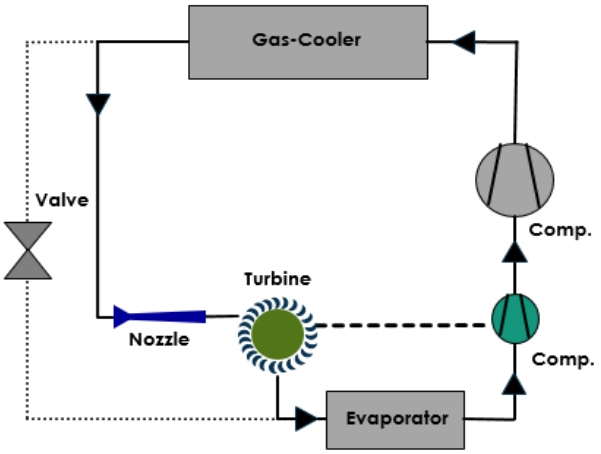

FIGURE 1: REFREGIRATION SYSTEM WITH TWO-PHASE TURBINE (CONTINUOUS LINE) REPLACING THE VALVE (DOTTED LINE)

This system is of a particular interest in summer operating conditions since it helps in gaining up to 30% of performance [2]. Various types of work-producing expansion devices have been studied for CO_2 such as volumetric or rotodynamic expanders/turbines [3],[4], but there is no commercially successful example of such devices. One of the reasons for this is the lack of a general method for designing such devices. The literature on the topic is very poor compared to that on single-phase turbines. This work aims to develop a design method for the specific case of the impulse rotodynamic turbines that should result in cheap devices compared to volumetric expanders. The work is focused on a rotodynamic impulse turbine whose stator is a two-phase nozzle placed in front of the impeller. Maximizing the efficiency of this nozzle is a necessary step to increase the overall performance of the system. To achieve this, it is useful to determine an optimum nozzle design corresponding to the maximal efficiency. This work first seeks to model the two-phase flow in a nozzle. A two-fluid model is developed and compared with similar cases from the literature. Then optimization method is presented. Finally, various CO_2 expansion cases are studied and the resulting optimized nozzle profiles are analyzed. Describing the flow using a two-fluid model combined with geometric optimization of a CO_2 nozzle is an innovative approach that has not yet been studied in the literature.

2. MATERIALS AND METHODS

2.1 Nozzle modeling

The challenge of modelling the flow inside the nozzle is to estimate the different mass, energy and momentum transfers during the phase change. A schematic diagram of the nozzle geometry and the various phase interactions is shown in figure (2).

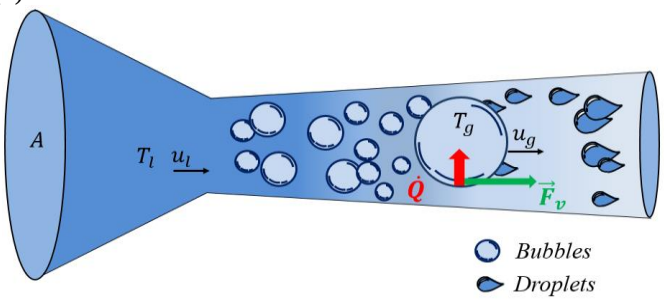

FIGURE 2: SCHEMATIC OF THE NOZZLE AND THE PHYSICAL PHENOMENA

Here we assume that the vapour phase and the liquid phase each have a different temperature and velocity. The modelling that follows will look at the interactions between these two phases. The exchanges considered will therefore be heat exchanges between the phases, frictional exchanges and material exchanges between the phases. These exchanges, modelled by transfer terms, will be integrated into the equations described below. We will also model as a function of the fraction of vapour or gas if these exchanges take place between droplets or bubbles. At the end of the nozzle, the fraction of gas being lower, we will consider bubbles and at the end of the nozzle we will consider droplets.

2.1.1 Governing equations

The model presented here uses a Eulerian-Eulerian approach to two-phase flow, applying conservation relations for each phase. In the stationary, one-dimensional case, these can be expressed as White [5]:

For the liquid phase:

$$\frac{\partial(\alpha_l \rho_l A u_l)}{\partial x} = A\Gamma_l \tag{1}$$

$$\frac{\partial(\alpha_l \rho_l A u_l^2)}{\partial x} + A\alpha_l \frac{\partial p}{\partial x} = A\left[\vec{F}_l + \Gamma_l u_i + \alpha_l \left(\frac{dp}{dx}\right)_{f,l}\right] \tag{2}$$

$$\frac{\partial\left(\alpha_l \rho_l A u_l\left(h_l + \frac{u_l^2}{2}\right)\right)}{\partial x} = A\left[UA_i(T_v - T_l) + \Gamma_l\left(h_i + \frac{u_l^2}{2}\right)\right] \tag{3}$$

For the vapour phase:

$$\frac{\partial(\alpha_v \rho_v A u_v)}{\partial x} = A\Gamma_v \tag{4}$$

$$\frac{\partial(\alpha_v \rho_v A u_v^2)}{\partial x} + A\alpha_v \frac{\partial p}{\partial x} = A\left[\vec{F}_v + \Gamma_v u_i + \alpha_v \left(\frac{dp}{dx}\right)_{f,v}\right] \tag{5}$$

$$\frac{\partial\left(\alpha_v \rho_v A u_v \left(h_v + \frac{u_v^2}{2}\right)\right)}{\partial x} = A\left[-UA_i(T_v - T_l) + \Gamma_v\left(h_i + \frac{u_i^2}{2}\right)\right] \tag{6}$$

Where p, is the pressure and α, ρ, u, are respectively the volume fraction, density, velocity of each phase. The cross-sectional area of the nozzle is defined by A. The thermophysical properties of the fluids utilized in this study were determined using the open-source software library CoolProp [6]. The terms to the right of the equalities are source terms, corresponding to the amount of mass, motion and energy exchanged between the phases. The mass transfer term at the interface between the phases uses a two-resistance model [7], [8], is expressed as follows: :

$$\Gamma_l = -\Gamma_v = \frac{\mathfrak{H}_l A_i (T_{sat} - T_l) + \mathfrak{H}_v A_i (T_{sat} - T_v)}{h_{lv}} \tag{7}$$

This expression will only be used for a comparison to White's model.

In the other cases we will assume that the vapor is in a saturated state, and mass transfer will be modelled by the following expression [9], [10] :

$$\Gamma_l = -\Gamma_v = \frac{h_c A_i (T_{sat} - T_l)}{h_{lv}} \tag{8}$$

The term involving the transfer of momentum includes the frictional force between phases at the interface. Its expression is as follows [7]:

$$\vec{F}_l = -\vec{F}_v = \frac{C_D}{8} A_i \rho_v |u_v - u_l|(u_v - u_l) \tag{9}$$

The term involving energy transfer involves U, which corresponds to the overall heat transfer coefficient, and is expressed as follows [5]:

$$U = \frac{1}{\mathfrak{H}_l} + \frac{1}{\mathfrak{H}_v} \tag{10}$$

If we use equation (8) instead of equation (7) to model mass transfer, the overall heat transfer coefficient becomes:

$$U = \frac{1}{h_c} \tag{11}$$

We also model pressure losses in the nozzle using the Bandel correlation [11], this empirical correlation can be used to estimate the pressure losses of a two-phase flow in a variable cross-section tube:

$$\begin{cases} \left(\frac{dp}{dx}\right)_{f,l} = \xi_l \frac{\dot{m}^2}{2\rho_l d} = A \\ \left(\frac{dp}{dx}\right)_{f,v} = \xi_v \frac{\dot{m}^2}{2\rho_v d} = B \end{cases} \tag{12}$$

$$with \begin{cases} if\ Re_l, Re_v \leq 1187 : \xi_l = \frac{64}{Re_l},\ \xi_v = \frac{64}{Re_v} \\ if\ Re_l, Re_v > 1187 : \xi_l = \frac{0.3164}{Re_l^{1/4}},\ \xi_v = \frac{0.3164}{Re_v^{1/4}} \end{cases} \tag{13}$$

$$\left(\frac{dp}{dx}\right)_{f,ph} = G(1 - \dot{x}_v)^{1/C} + B\dot{x}_v{}^C \tag{14}$$

$$with : \begin{cases} G = A + 2(B - A)\dot{x}_v \\ C = 3 \end{cases} \tag{15}$$

At the interface, empirical correlations are used to determine some of the magnitudes of source terms. Heat transfer coefficients are calculated using the following Ranz-Marshall correlation [4]:

$$Nu_v = \frac{h_v D}{k_v} = 2 + 0.6 Re_D^{\frac{1}{2}} Pr^{\frac{1}{3}} \tag{16}$$

$$with \begin{cases} Re_D = \frac{\rho_v |u_v - u_l| D}{\mu_v} \\ Pr_v = \frac{C_{p,v}\mu_v}{k_v} \end{cases} \tag{17}$$

Where k_v, μ_v, $C_{p,v}$, are, respectively, the thermal conductivity, viscosity, and specific heat capacity of the vapor. The diameter of liquid droplets is defined by D. Additionally, the Nusselt number of the liquid is defined as [5]:

$$Nu_l = \frac{h_l D}{k_l} = 6 \tag{18}$$

If we consider the expression of the mass transfer term from equation (8), then as proposed by Liao & Lucas we can use the Aleksandrov heat transfer coefficient [9]:

$$h_c = \frac{\lambda_l}{l_c}\left(\frac{12}{\pi^2} Ja^2 + \frac{1}{3\pi} Pe\right)^{1/2} \tag{19}$$

$$with \begin{cases} Ja = \frac{C_p \rho_l (T_l - T_{sat})}{\rho_v h_{lv}} \\ Pe = \frac{|u_v - u_l| l_c}{D_{T,l}} \end{cases} \tag{20}$$

The mean bubble diameter is related to the number of bubbles by the following relationship:

$$D_b = \left(\frac{6\alpha_v}{\pi N_b}\right)^{1/3} \tag{21}$$

Regarding the friction coefficient at the interface, it is determined using the following Schiller-Naumann correlation [7]:

$$C_D = \begin{cases} \frac{24}{Re_D}, & if\, Re_D \leq 0.1 \\ \max\left(0.44, \left(\frac{24}{Re_D}\right)(1 + 0.15 Re_D^{0.687})\right) & Otherwise \end{cases} \quad (22)$$

To determine which phase is exchanging and thus determine the direction of the various fluxes, the following condition is used [9]:

$$\begin{cases} if\ \ \Gamma_l < 0: \quad u_i = u_l \quad and \quad h_i = h_l \\ if\ \ \Gamma_l > 0: \quad u_i = u_v \quad and \quad h_i = h_v \end{cases} \quad (23)$$

The interfacial area between the phases A_i is modeled as follows [10] where a non-symmetric bubble to droplet transition model was explored:

$$\begin{cases} if\ \ \alpha_v < 0.3: \quad A_i = (6\alpha_v)^{2/3}(\pi N_b)^{1/3} \\ if\ \ \alpha_v > 0.7: \quad A_i = (6(1-\alpha_v))^{2/3}(\pi N_d)^{1/3} \end{cases} \quad (24)$$

It is assumed that at low vapor fractions there are only bubbles and that at high vapor fractions there are only drops.

2.1.2 Nozzle efficiency

The nozzle efficiency is calculated as follows[12]:

$$v_{isen} = \sqrt{2\left[\left(h_{in} + \frac{1}{2}{v_{mix}}^2\right) - h_{isen,out}\right]} \quad (25)$$

$$v_{mix} = \dot{x}_v u_v + (1 - \dot{x}_v) u_l \quad (26)$$

$$h_{mix} = \dot{x}_v h_v + (1 - \dot{x}_v) h_l \quad (27)$$

$$\eta_n = \frac{v_{mix}^2}{v_{isen}^2} \quad (28)$$

The nozzle efficiency value will subsequently be used to validate the model and to find a nozzle design capable of maximizing this value.

2.1.3 Numerical Resolution

Equations 1 to 6 form a system of equations that will be solved for each node. The division of the domain into nodes is shown in the following schematic:

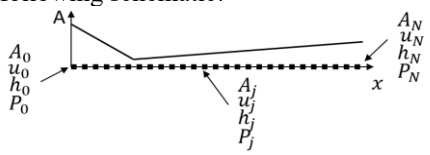

FIGURE 3: SCHEMATIC OF THE DIVISION OF THE DOMAIN INTO NODES

Here N is the total number of nodes, j, is an iteration between 0 and N. In a similar approach to the one of White [5] and Sagnes et al. [13], for a given pressure profile, the 6 unknowns of the system are $\alpha_v, A, u_v, u_l, h_v, h_l$, and can be expressed in the following form as [13]:

$$\frac{\partial X}{\partial x} - Y = 0 \quad (29)$$

Where X corresponds to the terms on the left-hand side of equations 1 to 6, and Y corresponds to the source terms on the right-hand side of the equations. Similar to Sagnes et al [13], at each node the values of the variables are initialized to first order from the previous values such as :

$$X_{j,ini} = X_{j-1} + \Delta x \frac{dX_{j-1}}{dx} \quad (30)$$

We solve this system using the 6 variable root optimizer in the SciPy library for Python [14]. This allows us to find the values of the 6 variables that minimize the residual resulting from subtraction (29). We use the linear mixture method, which employs a scalar estimate of the Jacobian [14]. The derivative of the matrix X and the pressure gradient are estimated using a second-order backward difference scheme.

The pressure profile is a model input and is estimated by a Bézier curve [15] with 5 control points P_i. This curve is a combination of Bernstein polynomials and is particularly effective for representing flat curves numerically. Its expression is as follows:

$$P(t) = \sum_{i=0}^{n} \binom{n}{i} (1-t)^{n-1} t^i . \mathrm{P}_i \quad where\ t \in [0;1] \quad (31)$$

This method of resolution in which the pressure profile is a given of the problem is chosen with an aim of carrying out a tool of dimensioning of the nozzle. Indeed, varying the control points of the Bézier curve would make it possible to cover a wide range of possible nozzle designs easily.

2.1.4 Model validation

As the mathematical model used in this work is designed to optimize geometries, its ability to predict geometrical features from literature case studies is used for validation.

First, the implementation of the model presented here is compared with White's [5] results for an expansion with R1233zd(E). The nature of the model he developed is very similar to the one presented here, notably in its assumption that the system is neither in thermal nor in mechanical equilibrium. White's model does not take into account the Bandel correlation [11] and the equations (8), (11), (19), (20), (24). White's model has itself been compared with Elliot's [16] model, which assumes that the system is in thermal equilibrium. A sensitivity study on the number of meshes is presented in the following table:

TABLE 1: SENSITIVITY STUDY ON THE NUMBER OF MESHES

Number of nodes :	η_n	$u_{l,out}$	$u_{v,out}$	$T_{l,out}$	$T_{v,out}$	$\alpha_{v,out}$
150	0.59	175.24	265.15	125.28	46.47	0.99
500	0.59	175.28	265.34	127.49	47.99	0.99
1000	0.59	175.30	265.35	127.50	48.04	0.99

Three different mesh numbers are tested, 250, 500 and 1000. The nozzle efficiency, η_n, the velocities of the different phases, their temperatures and the vapor volume fraction at the nozzle outlet are plotted against these mesh numbers We observe that the relative error of all these quantities between the cases with 250 and 1000 meshes is less than 1%. For the rest of the calculations, we will use the case with 250 meshes. The profiles of volume fraction, velocity, temperature, and cross-sectional area are presented in Figure (4). The profiles coincide well which validates the implementation of the model.

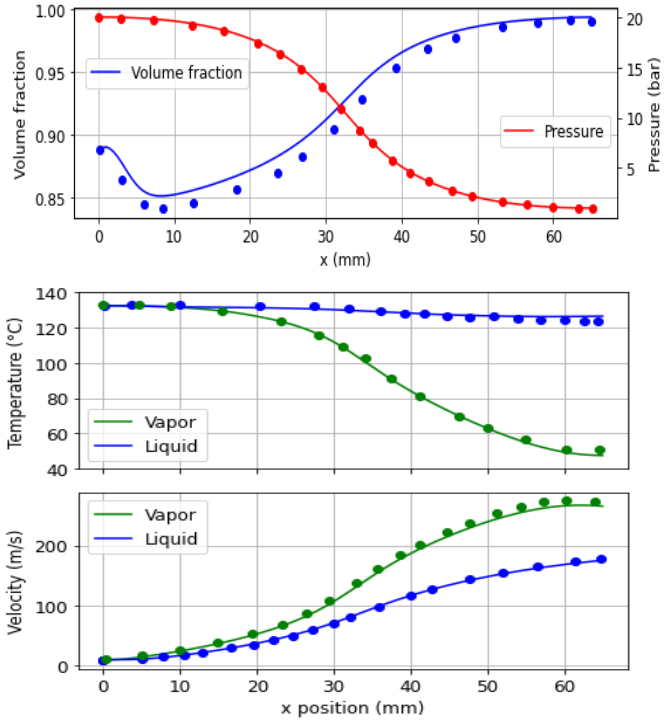

FIGURE 4: VALIDATION OF THE MODEL AGAINST RESULTS OBTAIN FROM WHITE [5] (●). THE PRESENT CASE IS FOR FORANE, WITH THE FOLLOWING OPERATING POINTS $P_{in} = 20\ bar,\ u_{in} = 10\ m/s,\ \dot{x} = 0.5,\ P_{out} = 1\ bar, N_d = 10^8$

The model is also compared with work by Zhang et al. [12], who studied two-phase expansion in the primary nozzle of a CO_2 ejector. The dimensions are similar to those experimentally tested by Nakagawa [17]. The pressure profile obtained by Zhang is reproduced by numerical optimization of Bézier control points. The operating points of the expansion in both cases are as follows : $P_{in} = 61\ bar, T_{in} = 293.65\ K, P_{out} = 14\ bar$, $\dot{m} = 0.02611\ kg/s$, $\alpha_0 = 0.01$. Moreover, in the model presented here, the heat transfer model of equation (8) and the interfacial area model of equation (24) were used because they have proved their worth to model a transcritical CO_2 ejector [9]. The number of droplets and bubbles is determined by an order of magnitude because it is not modelled in the work of Zhang et al. [12]. The order of magnitude is chosen according to the work of E. Ortego Sampedro [10], who studied expansion processes where the operating conditions are very similar to the present case: $N_b = N_d = 10^{15}$. The comparison is shown in figure (5).

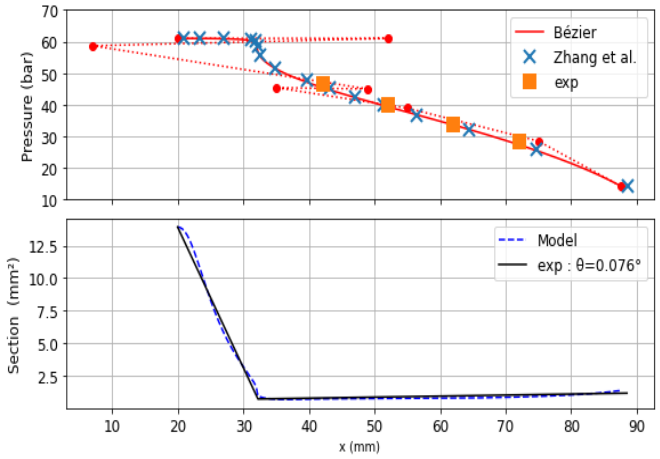

FIGURE 5: REPRODUCTION OF THE PRESSURE PROFIL OBTAIN BY DU ET ZHANG [12] WHIT A BEZIER CURVE WITH 8 CONTROL POINTS (●) AND SECTION OBTAIN. (EXP=DATA OBTAIN BY NAKAGAWA [17]).

We observe good predictions for the nozzle cross-section with a 5% error on the throat diameter. Moreover, one of the interests here is to estimate the nozzle efficiency value derived from relation (28). We obtain a nozzle efficiency of 92%, compared with 97.5% given by the CFD simulation from Zhang et al. [12].

The model is validated in various stages. Firstly, we reproduce White's model [5] to validate all the mathematical implementations of the resolution. This first stage confirms that the model works mathematically and numerically, which is the case, as we obtain almost similar results. We then decided to apply this model to the case of CO2 using Zhang's results [12]. This second step enables us to validate our model for CO2, since for the same operating and initial expansion conditions, we obtain an almost identical nozzle cross-section. This step validates the possibility of using a 1D model in such cases since the results are very closed to the results of Zhang's CFD model and also validates the inverse formulation used in this work. Finally, regarding the transcritical operation of the nozzle, the two-fluids formulation (cf. Section 2.1.1) and the interfacial transfer terms were validated by CFD [10] the values for Nb and Nd.

2.2 OPTIMISATION PROCESS

2.2.1 Optimization variables

The aim here is to develop a method for determining the nozzle profile that will maximize its efficiency, η_n, determined in equation (28). This is an optimization problem which will be solved by optimizing the control points of the pressure profile in equation (31). The coordinates of the control points, P_i, in the initial case proposed by White [5] are shown in figure (6):

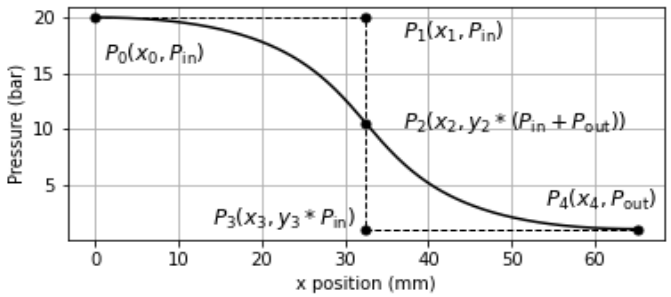

FIGURE 6: PRESSURE PROFILE AND VARIABLE COORDINATES OF BEZIER CURVE CONTROL POINTS

Each control point has 2 coordinates, the input and output points are fixed and the y_1 coordinate of point P1 is set to be equal to the input pressure. This choice was made to avoid positioning the nozzle throat at the start of the domain. So, the optimization variables are x_1, x_2, y_2, x_3, y_3. These co-ordinates are formalized as shown in Figure (5), which will allow optimization limits to be set later. Here the nozzle length is not an optimization variable. We are studying a compact nozzle.

2.2.2 Optimization Method

There are several varieties of optimization methods. We applied four optimization methods to the five control points of the Bézier curve. The four methods are Nelder-Mead optimization with minimize on ScyPy [14], differential evolution optimization on ScyPy [14], genetic algorithm optimization [18] and particle swarm optimization [19]. These optimizers make it possible to optimize several variables for a single objective function, which is nozzle efficiency. Their optimization methods are specific. Their specificity are detailed in their associated documentation. A brief comparison of these methods is carried out to select the most suitable for the problem under consideration. The results of the different methods are presented in the figure (7) as the efficiency of the nozzle as a function of the number of iterations for the R1233zd case. The expansion operating points and the initial pressure profile are those taken from White's work [5], which are also described in section 2.1.3. The values of the optimization parameters are taken by default.

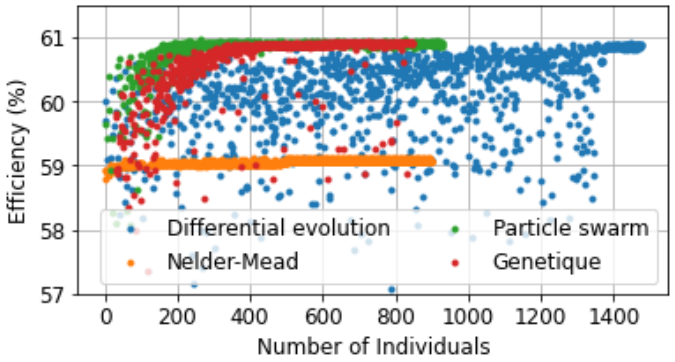

FIGURE 7: COMPARAISON OF THE RESULTS OBTAINED FOR FOUR OPTIMISATION METHODS

The individuals are all the pressure profiles tested by the optimization method, this denomination is specific to genetic algorithms. An individual corresponds to a combination of control points tested, i.e. one optimization iteration. Initially, the pressure profile used by White gave an efficiency of 59%, while the particle swarm method, the genetic algorithm method and the differential evolution method give a maximum efficiency of 61%. The Nelder-Mead method [20] achieves a maximum efficiency of 59%, mainly because this method determines a local maximum , in fact the optimum depends on the initial pressure profile . The method does not allow us to cover a wide range of possible profiles. However, it can be effective if used in conjunction with another method. In addition, the genetic algorithm method is the fastest for a similar number of iterations to that of the other methods. The differential evolution method and the particle swarm method requires more iterations to determine the optimum. We will therefore choose the genetic algorithm optimization for the rest of the calculations

For this method, the determining parameters are the number of individuals, the number of generations and the mutation probability. The total number of individuals will affect the chances of finding the optimum value and the length of the calculation. For this preliminary study, we are not going to carry out an exhaustive sensitivity study of these parameters on the solution obtained. We will choose a population size of 30 individuals for 30 generations, i.e. a total number of 900 individuals. For these values we reach a plateau on the curve of the evolution of efficiency as a function of the number of individuals. At this plateau, the variation in efficiency varies very little, which indicates that we are very close to the optimum value. The mutation probability is set at 0.7, which controls the intensity with which an individual's genes will be modified during the mutation phase. The pressure profiles generated are considered to make physical sense when the discretization element of length Δx, is always positive and the numerical derivative of pressure $\Delta P/\Delta x$, is always negative. Otherwise, the nozzle efficiency is set close to 0. This constraint in necessary when using Bezier curves in order to avoid non monotonic pressure profiles.

2.3 OPERATING POINTS

We will now study four different expansions more in detail, they are represented in an enthalpy diagram in the following figure (8), the numbering of cases 3,6,9,11 is derived that proposed by Haida et al. [21]. These expansions lie within the range of the operating optimums for CO_2 refrigeration cycles. These optimums have been modelled by Zhang et al [2] . These optimums are calculated for the temperature at which the fluid enters the expansion process. This is determined by the ambient temperature outside the refrigeration system.

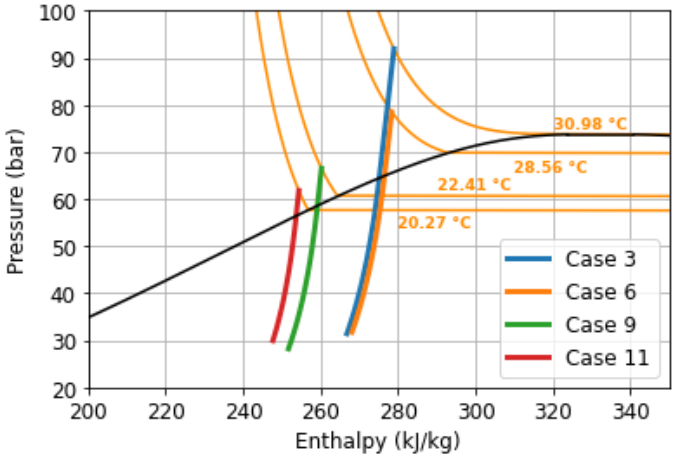

FIGURE 8: OPERATING POINTS OF STUDYING EXPANSIONS

The expansions treated in this work are represented in the figure (8), in the isentropic case, which corresponds to the ideal case. The model developed here can be used to evaluate the entropy losses generated by the different energy and mass transfers between the phases. The aim of the remainder of this work will be to find nozzle design conditions that are as close as possible to the isentropic case.

An important parameter of the model is its sensitivity to the number of bubbles and droplets. These parameters have been studied by E. Ortego Sampredro [10] in the case of the primary nozzle of a CO_2 ejector experimentally studied by Haida et al. [21]. E. Ortego Sampedro estimated the number of bubbles and droplets by validating specific flow values with experimental results. These results for the four considered expansion and operating points are presented in the following table (2):

TABLE 2: OPERATING POINTS FOR EXPANSIONS TESTED [21].

Case n° :	P_{in} (bar)	T_{in} (°C)	P_{out} (bar)	$\dot{m}\ (\frac{kg}{s})$	N_b/N_d
3	91.91	30.98	31.41	0.095	$7.10^{14}/4.10^{15}$
6	78.45	28.56	31.72	0.073	$3.10^{15}/3.3.10^{13}$
9	66.51	22.41	28.21	0.072	$2.2.10^{15}/5.10^{13}$
11	61.79	20.27	29.93	0.072	$1.7.10^{15}/1.10^{12}$

These results are derived from CFD modelling of two-phase CO_2 ejectors in which the experimentally measured primary and suction mass flow rates are found by the calibration of the number of bubbles and the number of droplets. This calibration is notably permitted by the particular formulation of the interfacial surface density described by equation (24).

A schematic diagram of the ejector is shown in the following figure (9). Here we are interested in the primary nozzle of the ejector. The primary nozzle is the motive nozzle that drives the ejector performances and observes a trans-critical expansion.

It can be mentioned that the optimization for turbines nozzle would also be useful for ejectors.

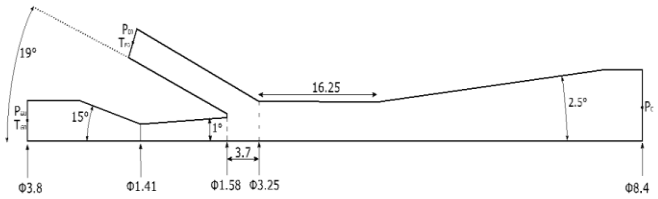

FIGURE 9: DIAGRAM OF THE EJECTOR [21] USED TO CALIBRATE THE MODEL [10].

3. RESULTS AND DISCUSSION

The optimization results by genetic algorithm obtained for the four operating conditions are presented in figure (10). The initial pressure profiles are generated randomly.

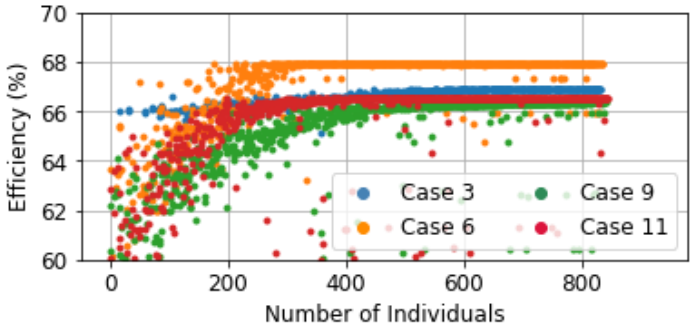

FIGURE 10: GENETIC ALGORITHME OPTIMISATION RESULTS FOR THE FOUR STUDYING EXPANSIONS

The optimum efficiencies for cases 3, 6, 9 and 11 are respectively 67%, 68%, 66% and 67%. These values have on average 8% efficiency points above the least efficient cases tested by the optimizer. This value represents the potential gain achievable by this optimization under the given conditions.

In the following, we will only look at the optimum cases, which correspond to the pressure profiles whose control points are shown in the table (3) below:

TABLE 3: COORDINATES OF THE CONTROL POINTS ASSOCIATED WITH THE OPTIMUM PRESSURE PROFILES

Case n° :	$x_1(mm)$	$x_2(mm)$	y_2	$x_3(mm)$	y_3
3	2	2	0.51	2.00	1.14
6	2	2	0.48	5.63	1.47
9	2	2	0.48	11.33	1.25
11	2	2	0.46	10.73	1.37

The modelling of the nozzle starts at the position of 2 mm because before the convergent part there is a constant section from 0 to 2mm in a similar way to the nozzle presented by Sampedro [21]. It is assumed that there is no pressure variation along this length. The pressure profiles associated with these control points are as follows:

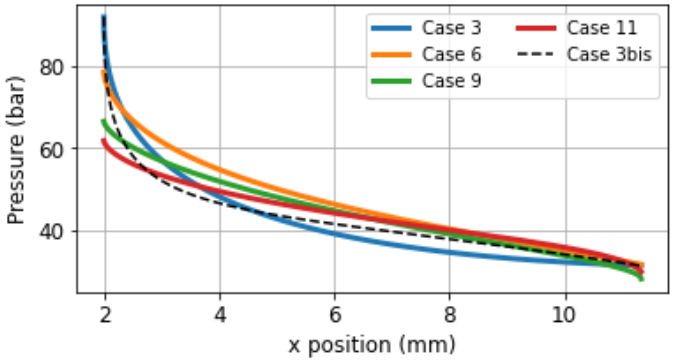

FIGURE 11: OPTIMUM PRESSURE PROFILES

The optimal nozzle geometries for the studied cases are shown in figure (12), the diameter and position of the throat and the output diameter are also indicated:

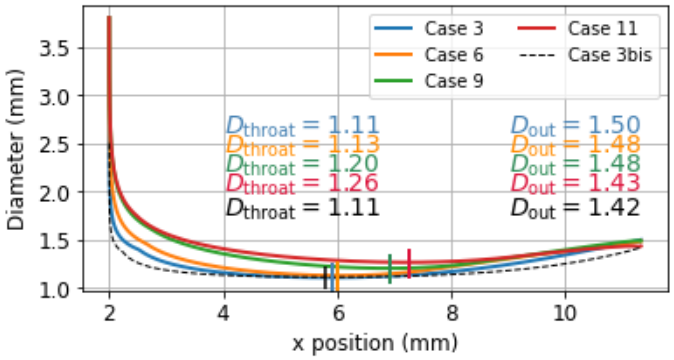

FIGURE 12: OPTIMUM NOZZLE DIAMETERS (THE POSITION OF THE THROAT IS MARKED BY A DASH)

These profiles have several interesting characteristics. First, the final throat diameter is close to the initial one, and the section variation is very smooth at this point. This suggests that the initial sharp section variation (transition from 15° to 1°) is not optimal. Also, this results in a convergent that tends to look like a straight pipe with a diameter way smaller than the inlet diameter. The optimizer suggests a smooth variation of diameter between the inlet and the throat, probably because this is the best way to limit the pressure drops in cases of sharp diameter variations, as suggested by Idel'chik [22]. Probably using a smooth profile close to the throat is more important than having a smooth profile close to the inlet because velocities are way higher at the throat than at the inlet. Elliot [24] has also obtained a vertical slope at the entrance to the optimum nozzle profile. However, he asserts that in practice a maximum slope of 20° for the convergent nozzle is possible. In order to test his experimental device, Elliot [24] proposes replacing the optimum convergent nozzle, which is too vertical, with a convergent nozzle with a 20° inclination tangent to the optimum profile. However, the maximum angle of 20° is not explained. In order to understand the effect of the inlet cross-section on the nozzle efficiency, a case 3 bis is carried out, which differs from case 3 only in the size of the inlet diameter, which is initialised here at 2.5 mm. An efficiency of 67% is obtained for this case 3 bis, which is not significantly different from case 3.

The geometry of the nozzles in Case 9 and Case 11 are very similar, as are the operating points of these two expansions. It is difficult to isolate the effect of one of the inlet conditions on one of the nozzle's geometric characteristics. A sensitivity study on the inlet temperature, inlet pressure, outlet pressure or flow rate could give rise to future work. Eventually, simultaneous optimization for various operating points could be performed. Also, a detailed analysis of the frequency of operating conditions could be added as a design parameter when studying a specific usage case. Moreover, a comparison of the optimized nozzle of case 11 with the original nozzle [21] has been performed with CAD software and is presented in the following figure (13):

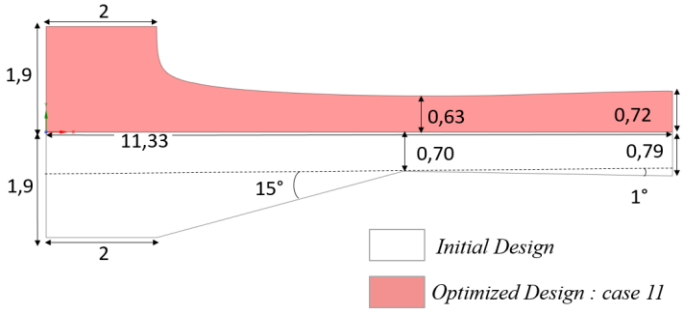

FIGURE 13: COMPARAISON OF THE OPTIMIZED NOZZLE OF CASE 11 WITH ORIGINAL NOZZLE [21] (DIMENSIONS IN mm)

The velocities of the different phases of the flow are shown in figure (14):

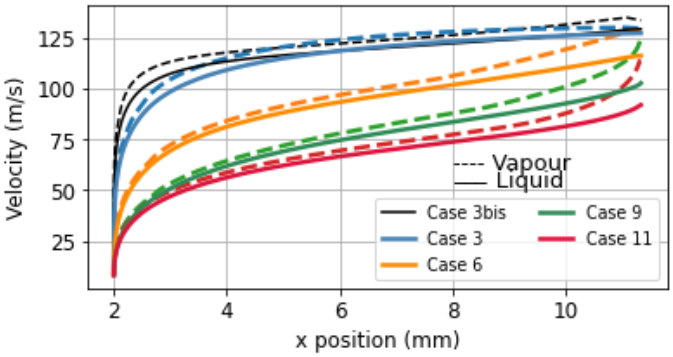

FIGURE 14: VELOCITY PROFILE OF THE VAPOUR PHASE (DOTTED LINE) AND THE LIQUID PHASE (CONTINUOUS LINE) FOR THE DIFFERENT CASES

One of the great strengths of the two-fluid model is its ability to determine the velocity of the fluid and the velocity of the gas separately. Here, in case 11, the velocity slip is 25 m/s, which is not insignificant, particularly with a view to the design of rotating parts at the nozzle outlet. We can see that the velocity at the nozzle outlet is higher in cases where the inlet pressure and temperature are higher.

The variation of the volume fraction as a function of the nozzle position is also shown in the following figure (15):

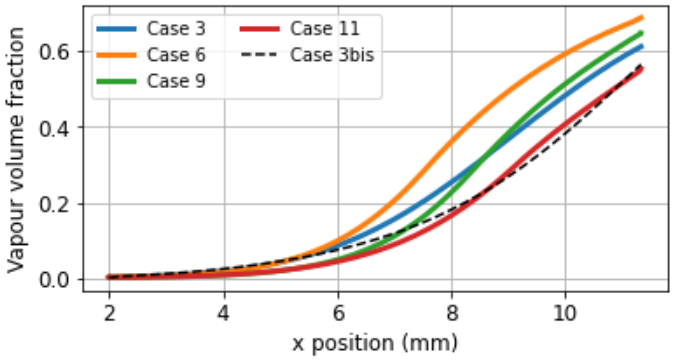

FIGURE 15: VAPOUR VOLUME FRACTION FOR THE DIFFERENT STUDIED CASES

Concerning the volume fractions, a volume fraction of 0.003 is used as the initial condition. This value is the same for the different expansion stages and is chosen so as to be close to 0, but not zero, in order to avoid division by zeros in the model equations.

The enthalpy of the process can also be represented as a function of pressure, compared with the isentropic case. This is shown in the following figure (16):

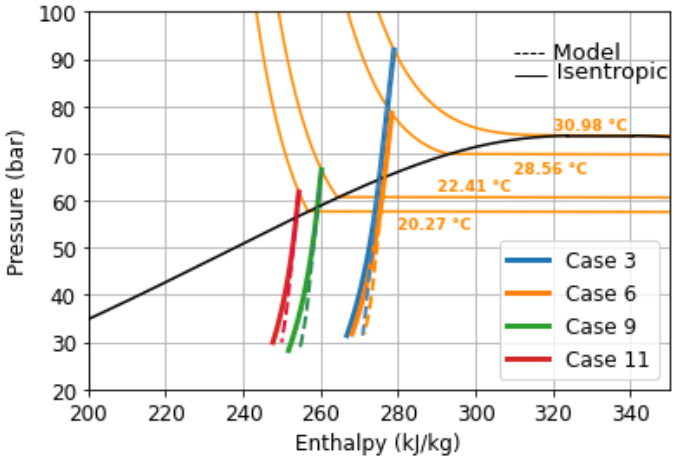

FIGURE 16: ENTHALPY-PRESSURE DIAGRAM WITH MODELLED MIXING ENTHALPY (DOTTED LINE) AND ISENTROPIC EXPANSION (SOLID LINE) FOR THE DIFFERENT CASES

The enthalpy variation of the mixture between the fluid and the vapour is calculated from equation (27), and is therefore the sum of the enthalpy of the gas and the liquid weighted by the mass fraction. This representation allows us to understand the difference between an isentropic expansion (continuous line) and the modeled case, which takes into account the effects of non-equilibrium (dotted line). The optimization stage of the section enables us to get closer to the isentropic case. Given that the expansion process is a major source of energy loss [1], the sizing tool proposed here could help to improve the efficiency of certain thermodynamic cycles.

This two-fluid model has the particularity of modeling each of the interacting phases. This is not always the case, and in some models, only one fluid is considered, which is a mixture of two phases. This gives access to a greater number of thermal-hydraulic parameters and, therefore, greater control. We can think in particular of the differences in speed between the phases; knowing which of the two phases has the greater speed and in what proportion will be essential if we want to couple the nozzle to a rotating machine. Particularly in the design of the rotor blades. This access to many thermal-hydraulic parameters also results in a finer representation of the physics of the flow, in particular by taking exhaustive account of the interactions between phases, i.e., the transfer of mass, energy and momentum. Furthermore, this model requires very little computing power, just 1m 30 for a profile calculation, which is practical for the optimization stage, which lasts several hours. It can also be adapted to other fluids. Finally, this modeling takes its strength from its construction by inverse formulation. The possibility of imposing a pressure profile gives us greater control over the physics of the process by allowing us to control the properties of the fluids leaving the expansion. This is particularly interesting for a dimensioning tool.

It should be remembered that the work presented here is conditional on the primary ejector nozzle, and we have chosen to start from an existing design in order to optimize it. It is for this reason that we keep the length of the primary nozzle constant. However, we note that in the case of the nozzle studied by Zhang, the efficiency is of the order of 90% for a much longer nozzle (88mm) compared with 67% for ejector primary nozzles, which are smaller (11mm). So it seems important to increase the length of the nozzle to increase its efficiency. This is not necessarily possible for ejectors. So the choice of geometric optimization parameters depends on the application. In this case, we chose the ejector application largely because we had preliminary CFD work enabling us to match the number of bubbles and droplets with experimental results, thus adding value to our own results.

Furthermore, the present work does not attempt to model the coalescence or rupture of droplets. The hypotheses assume a constant number of droplets and bubbles and a constant diameter. It is assumed that, above a certain volume fraction, it is either the droplets or the bubbles that dictate the exchange surface between the phases. Physically, the effects of non-equilibrium will reduce the mixing speed compared with the isentropic case. Part of the fluid's kinetic energy will be used for heat transfer, friction between phases and friction with the wall, which will reduce efficiency, according to relation (28). The efficiency value will therefore depend in part on the ability to model these non-equilibrium phenomena accurately; for example, we know that the efficiency depends a lot on Nd as suggested by [23]. Since these were calibrated on CO_2 ejector data, supplementary exploration is required to validate these aspects of the model. In particular, it would be very useful to perform CO_2 trans-critical nozzle efficiency measurements. Besides, energy loss terms could be analyzed and compared in order to quantify their respective importance. The optimization stage focuses on finding the optimum geometry that minimizes these non-equilibrium effects. The influence of geometry can be physically interpreted by the nozzle's ability to accompany the expansion process.

4. CONCLUSION

The present work proposes a genetic optimization method for maximizing the efficiency of two-phase CO_2 nozzles. This method is based on the optimization of Bézier control points using a genetic algorithm and a 1D two-fluid model. The optimizer leads to efficiencies gains between 3% and 9%. Following this preliminary work, the next steps will be to validate the optimum designs using CFD modelling. In addition, it would be interesting to assess the influence of the nature of the fluid on nozzle efficiency. Analyses of the effect of the mass transfer model on efficiency will also be carried out. Finally, studies will be carried out on the sensitivity of the expansion operating points and the inclusion of manufacturing constraints in the optimization process will be added.

REFERENCES

[1] H. K. Ersoy et N. Bilir, « Performance characteristics of ejector expander transcritical CO 2 refrigeration cycle », *Proceedings of the Institution of Mechanical Engineers, Part A: Journal of Power and Energy*, vol. 226, nº 5, p. 623-635, août 2012, doi: 10.1177/0957650912446547.

[2] Z. Zhang, H. Wang, L. Tian, et C. Huang, « Thermodynamic analysis of double-compression flash intercooling transcritical CO2 refrigeration cycle », *The Journal of Supercritical Fluids*, vol. 109, p. 100-108, mars 2016, doi: 10.1016/j.supflu.2015.09.002.

[3] L. Hays et J. J. Brasz, « A Transcritical CO2 Turbine-Compressor », p. 8, 2004.

[4] S. Singh, A. Singh, et M. S. Dasgupta, « CFD Modeling of a Scroll Work Recovery Expander for Trans-critical CO 2 Refrigeration System », *Energy Procedia*, vol. 109, p. 146-152, mars 2017, doi: 10.1016/j.egypro.2017.03.081.

[5] M. T. White, « Investigating the wet-to-dry expansion of organic fluids for power generation », *International Journal of Heat and Mass Transfer*, vol. 192, p. 122921, août 2022, doi: 10.1016/j.ijheatmasstransfer.2022.122921.

[6] I. H. Bell, J. Wronski, S. Quoilin, et V. Lemort, « Pure and Pseudo-pure Fluid Thermophysical Property Evaluation and the Open-Source Thermophysical Property Library CoolProp », *Ind. Eng. Chem. Res.*, vol. 53, nº 6, p. 2498-2508, févr. 2014, doi: 10.1021/ie4033999.

[7] « 113AnsysCFXSolverTheoryGuide-1.pdf ».

[8] H. Städtke, *Gasdynamic Aspects of Two-Phase Flow: Hyperbolicity, Wave Propagation Phenomena, and Related Numerical Methods*, 1re éd. Wiley, 2006. doi: 10.1002/9783527610242.

[9] Y. Liao et D. Lucas, « 3D CFD simulation of flashing flows in a converging-diverging nozzle », *Nuclear Engineering and Design*, vol. 292, p. 149-163, oct. 2015, doi: 10.1016/j.nucengdes.2015.06.015.

[10] E. O. Sampedro, « A Non Symmetric Interfacial Area Density Formulation for Transcritical CO2 Ejectors », 2021.

[11] H. Müller-Steinhagen et K. Heck, « A simple friction pressure drop correlation for two-phase flow in pipes », *Chemical Engineering and Processing: Process Intensification*, vol. 20, nº 6, p. 297-308, nov. 1986, doi: 10.1016/0255-2701(86)80008-3.

[12] Q. Du et D. Zhang, « Numerical Investigation on Flow Characteristics and Aerodynamic Performance of a 1.5-Stage SCO2 Axial-Inflow Turbine with Labyrinth Seals », *Applied Sciences*, vol. 10, nº 1, p. 373, janv. 2020, doi: 10.3390/app10010373.

[13] P. Sagnes et P. Gillant, « Calcul du profil de tuyères supercritiques détendant des liquides saturants ou des mélanges liquide-vapeur », *La Houille Blanche*, vol. 70, nº 3-4, p. 247-254, mars 1984, doi: 10.1051/lhb/1984016.

[14] « Virtanen, P., Gommers, R., Oliphant, T. E., Haberland, M., Reddy, T., Cournapeau, D., … SciPy 1.0 Contributors. (2020). SciPy 1.0: Fundamental Algorithms for Scientific Computing in Python. Nature Methods, 17, 261–272. https://doi.org/10.1038/s41592-019-0686-2 ».

[15] J.-P. Bécar et J. Vareille, « Une histoire de géométrie polaire brûlante d'actualité », 2011.

[16] D. G. Elliot, « Theory and tests of two-phase turbines », Jet Propulsion Lab., Pasadena, CA (USA); National Aeronautics and Space Administration, Washington, DC (USA), DOE/ER-10614-1; JPL-PUB-81-105, mars 1982. doi: 10.2172/5346135.

[17] M. Nakagawa, M. S. Berana, et A. Kishine, « Supersonic two-phase flow of CO2 through converging–diverging nozzles for the ejector refrigeration cycle », *International Journal of Refrigeration*, vol. 32, nº 6, p. 1195-1202, sept. 2009, doi: 10.1016/j.ijrefrig.2009.01.015.

[18] « Félix-Antoine Fortin, François-Michel De Rainville, Marc-André Gardner, Marc Parizeau and Christian Gagné, "DEAP: Evolutionary Algorithms Made Easy", Journal of Machine Learning Research, pp. 2171-2175, no 13, jul 2012. »

[19] L. James V. Miranda, « PySwarms: a research toolkit for Particle Swarm Optimization in Python », *JOSS*, vol. 3, nº 21, p. 433, janv. 2018, doi: 10.21105/joss.00433.

[20] F. Gao et L. Han, « Implementing the Nelder-Mead simplex algorithm with adaptive parameters », *Comput Optim Appl*, vol. 51, nº 1, p. 259-277, janv. 2012, doi: 10.1007/s10589-010-9329-3.

[21] M. Haida *et al.*, « An Object-Oriented R744 Two-Phase Ejector Reduced-Order Model for Dynamic Simulations », *Energies*, vol. 12, nº 7, p. 1282, avr. 2019, doi: 10.3390/en12071282.

[22] « Handbook of Hydraulic Resistance. ».

[23] E. Ortego Sampedro, F. Breque, et M. Nemer, « Two-phase nozzles performances CFD modeling for low-grade heat to power generation: Mass transfer models assessment and a novel transitional formulation », *Thermal Science and Engineering Progress*, vol. 27, p. 101139, janv. 2022, doi: 10.1016/j.tsep.2021.101139.

[24] D.G. Elliot, E. Weinberg, « Acceleration of Liquids in Two-Phase Nozzles », 1968.

